View metadata, citation and similar papers at core.ac.uk

brought to you by CORE

provided by DSpace at VU

Visualization of novel flux dynamics in $YBa_2Cu_3O_{7-x}$ thin films with antidots

This article has been downloaded from IOPscience. Please scroll down to see the full text article.

2001 Europhys. Lett. 54 682

(http://iopscience.iop.org/0295-5075/54/5/682)

View the table of contents for this issue, or go to the journal homepage for more

Download details:
IP Address: 130.37.129.78
The article was downloaded on 02/08/2011 at 07:33

Please note that terms and conditions apply.

EUROPHYSICS LETTERS 1 June 2001

Europhys. Lett., **54** (5), pp. 682–687 (2001)

Visualization of novel flux dynamics in $YBa_2Cu_3O_{7-x}$ thin films with antidots

R. Surdeanu[1], R. J. Wijngaarden[1], R. Griessen[1], J. Einfeld[2] and R. Wördenweber[2]

[1] *Division of Physics and Astronomy, Faculty of Sciences, Vrije Universiteit De Boelelaan 1081, 1081 HV Amsterdam, The Netherlands*

[2] *Institut für Schicht- und Ionentechnik (ISI) - Forschungszentrum Jülich, Germany*

(received 22 September 2000; accepted in final form 19 March 2001)

PACS. 74.60.Ge – Flux pinning, flux creep, and flux-line lattice dynamics.
PACS. 74.80.-g – Spatially inhomogeneous structures.
PACS. 74.76.Bz – High-T_c films.

Abstract. – Using magneto-optical visualization, individual 2 μm diameter antidots (circular holes) in $YBa_2Cu_3O_{7-x}$ thin films are clearly observed. These antidots are found to act at low temperature as very strong pinning centres. Flux penetration takes place along the lattice vectors of the antidot lattice. Both commensurate and incommensurate channels are observed as well as hopping between channels, in agreement with numerical simulations. Surprisingly, even for these large ($r/\lambda \simeq 7$) antidots the trapped flux is in agreement with previous theoretical work for small ($r \ll \lambda$) antidots.

The phase diagram of vortex matter in high-T_c superconductors is very rich and, in addition, can be strongly modified by the nature and spatial distribution of the defect structures present in the samples. In this context, artificially created random columnar defects have been extensively studied [1]. Recently, line defects with short-range correlation were shown [2] to be responsible for the high critical currents in thin film $YBa_2Cu_3O_{7-x}$ samples. In this letter, we focus on the influence of a perfect lattice of strongly pinning large antidots, *i.e.* holes patterned in a thin-film superconductor.

The interaction between vortices and such a hole was first studied theoretically by Mkrtchyan and Schmidt (MS) [3], who predicted the creation of a multi-quanta vortex, with a maximum number of trapped flux determined by the ratio between the radius of the cavity r (with $r \ll \lambda$, the penetration depth) and the coherence length ξ. Although the formation of flux line lattices of multi-quanta vortices is energetically unfavorable, the creation of antidots with a rather large radius ($r \gg \xi$, $r \simeq \lambda$) can stabilize multi-quanta vortices, as demonstrated in experiments on Pb and WGe films [4, 5], Pb/Ge multilayers [6–9], Pb/Cu bilayers [10] and vanadium [11] thin films. From magnetization measurements it was claimed [7] that the pinning properties of an antidot lattice are fully controlled by the ratio r/ξ, in agreement with the MS model. Numerical simulations of Reichhardt *et al.* [12–15] provide insight in the microscopic processes governing the interaction of vortices and pinning sites and predict

© EDP Sciences

intriguing novel flux flow phases in the dynamics of driven vortex lattices interacting with a square array of pinning sites. One of the new dynamic phases, in a region labelled IV in their work [14], occurs at larger driving forces and is characterized by an entirely 1-dimensional flow pattern with vortices flowing along the pinning rows. The channel pattern consists of two types: *commensurate* and *incommensurate* channels. The latter are created by the presence of additional vortices on some of the channels. Those additional mobile vortices give rise to "flux solitons" [14] that are penetrating at a faster speed than the "ordinary" vortices, although their propagation is still confined to the 1-dimensional channels.

Using our high-resolution magneto-optic (MO) technique [16], we visualize and investigate these novel structures, and find a number of remarkable results.

The $YBa_2Cu_3O_{7-x}$ thin films used for this investigation are deposited using a high-pressure on-axis magnetron-sputtering technique on CeO_2 buffered sapphire, with a thickness of 30 and 150 nm for CeO_2 and $YBa_2Cu_3O_{7-x}$, respectively [17]. The critical temperature for these films is $T_c = 88\,\mathrm{K}$, while at the temperature of measurement $\xi = 1.8\,\mathrm{nm}$ and $\lambda = 140\,\mathrm{nm}$. The antidot structure in the film is created by optical lithography and dry etching [18]. The antidot triangular lattice occupies an area of $9 \times 9\,\mathrm{mm}^2$ and consists of antidots of $2\,\mu\mathrm{m}$ diameter spaced at $10\,\mu\mathrm{m}$. The total area of the $YBa_2Cu_3O_{7-x}$ film is $10 \times 10\,\mathrm{mm}^2$, such that there is an antidot-free band of 0.5 mm width at the edge of the film.

The MO setup produces a two-dimensional image of the local magnetic field, where high fields are imaged as brighter regions, while dark regions are the field-free regions. The magnification used in this work is such that 1 pixel corresponds to $0.7\,\mu\mathrm{m}$. Typical exposure times are 1–10 s.

Figure 1(a) is a typical image recorded at $T = 8\,\mathrm{K}$ after zero-field cooling and application of 37 mT external field. The edges of the film are parallel to the edges of the image. The field of view is situated close to the center of the film and images are recorded every 1 mT. For an external field larger than 17 mT the flux front enters the field of view. In the first stage, vortices enter the superconductor at the edge of the sample, in the region without antidots. As soon as the flux front reaches the first antidots, the interaction between magnetic flux lines and antidots occurs as predicted by Mkrtchyan and Schmidt [3], with a first regime in which the vortices fill the antidots, until the saturation value for trapped flux quanta, $n_{\mathrm{sat}} = r/(2\xi(T))$, where r is the radius of the antidot, is reached. In our case this saturation value is $n_{\mathrm{sat}} = 280 \times \Phi_0$, where $\Phi_0 = h/2e$ is the flux quantum. A vortex lattice of multi-quanta vortices is formed, matching the antidot lattice, with two types of multi-quanta vortices: i) the unsaturated antidots situated near the flux front, containing less than n_{sat} vortices, and ii) the saturated antidots, containing $280 \times \Phi_0$.

We focus now on a quantitative analysis of the field trapped in the antidots. The total field in one antidot, or the number of trapped vortices, can be calculated by integrating the field over the area of one antidot after subtraction of the overall gradient in the induction. For the direction AA′ indicated in fig. 1(a) the result of this procedure is shown in fig. 1(b). Each of the antidots on the AA′ line accommodates a constant number of flux quanta $\simeq 280 \times \Phi_0$. The equivalent trapped field is shown on the right y-axis. This graph shows that the antidots along AA′ are situated in the saturated region of the sample, at this particular field. Despite the fact that vortices are moving, the number of flux quanta in the antidots stays the same. Although one expects from theory that in this area all the dynamics of vortices is such that once the antidots reach saturation, the moving vortices will be only the interstitial Φ_0-vortices, fig. 1(a) shows a rather intriguing feature: the appearance of incommensurate channels (where the average vortex density is larger than $280 \times \Phi_0$/antidot) in the vortex motion, as predicted in numerical simulations [14]. Those channels occur along only some of the rows of antidots, for example the ones indicated by the lines BB′ and CC′. In these channels the "excess" vortices

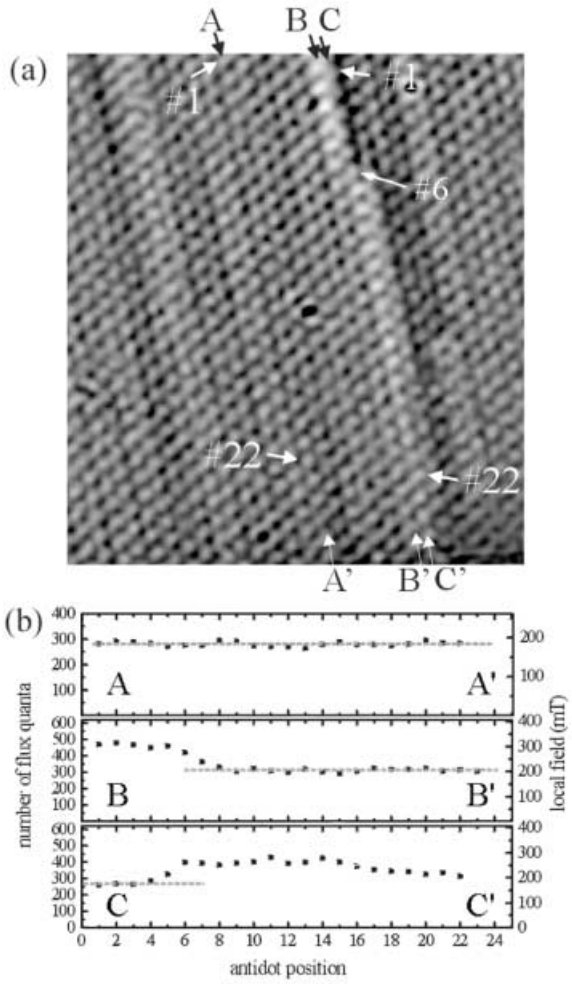

Fig. 1

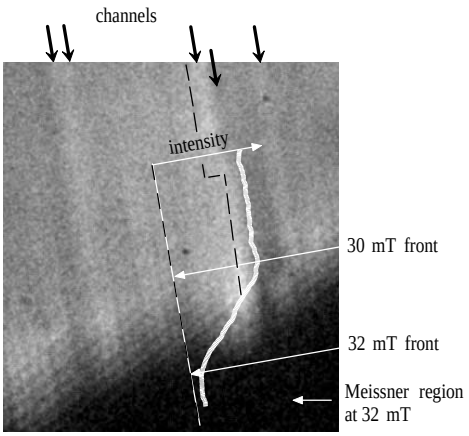

Fig. 2

Fig. 1 – (a) Magneto-optical image near the center of the sample recorded at $T = 8\,\mathrm{K}$ and 37 mT applied external field. The field of view is $210 \times 210\,\mu\mathrm{m}^2$. The flux trapped by the antidots appears as bright spots. AA′ indicates a commensurate channel, BB′ and CC′ two incommensurate channels. Hopping of vortex discommensurations between channel BB′ and CC′ is visible at the antidot #6. (b) Spatial variation of the number of flux quanta (on the left axis) and the local magnetic field (the right axis) at the positions of the antidots along AA′, BB′ and CC′. The position of the first and the last antidot of each channel is indicated by a white arrow. The constant trapped flux in the antidots along AA′ proves that AA′ is a commensurate channel. The hop from channel BB′ to CC′ is clearly visible at position # 6 of channel BB′.

Fig. 2 – Difference between the recorded MO images at $T = 8\,\mathrm{K}$ and applied external field of 32 mT and 30 mT, respectively. The field of view is $210 \times 210\,\mu\mathrm{m}^2$. There are three distinguishable regions: a Meissner region in the lower part of the figure, a region of constant field (the upper part) and, in between, a region where the multi-quanta vortex lattice is visible. Those three regions are separated by two fronts: one at the boundary of the Meissner state which represents the flux front at 32 mT applied field, and one visible as a brighter line, representing the front at 30 mT. The fact that the upper part of the image does not exhibit any structure demonstrates that the number of quanta per antidot remains constant (*i.e.* equal to their saturation value n_{sat}).

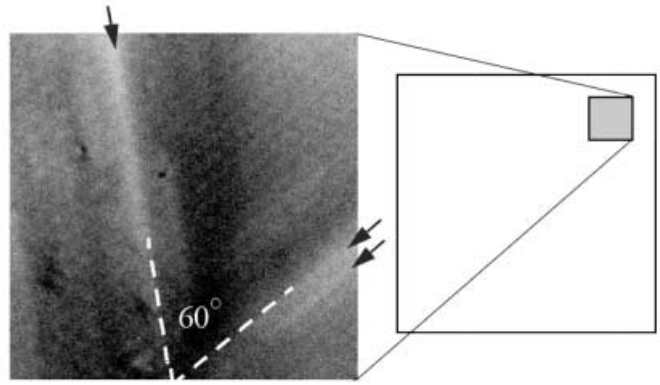

Fig. 3 – Magneto-optical image taken near one of the corners of the sample (position schematically indicated in the right part of the image) at $T = 7\,\mathrm{K}$ and applied field of 23 mT. The schematic drawing is not to scale. The field of view is $130 \times 130\,\mu\mathrm{m}^2$. The channels of easy vortex penetration are visible for both edges of the sample, with an angle of 60° between each other.

exhibit a 1-dimensional channel flow motion, in which the vortices are confined along the pinning rows defined by one of the triangular antidot lattice directions. Sometimes, vortices can also "hop" from one channel to another, in vortex bundles or discommensurations that advance further along the new "host" channel. One of these "hops" can be distinctly seen in figs. 1(a) and (b), between channels BB′ and CC′ at the position of antidot No. 6.

In order to gain more insight in the variations of the flux quanta distribution, we used a difference image technique. By subtracting the MO image taken at 30 mT from that taken at 32 mT, one obtains the difference image shown in fig. 2. The overlay shows an intensity scan along the black-and-white dashed line. There are three distinguishable regions: a Meissner region in the lower part of the figure (intensity is close to zero), a region of constant difference field (the upper part) and, in between, a region where the multi-quanta vortex lattice is visible (intensity is continuously increasing). Those three regions are separated by two fronts: one at the boundary of the Meissner state which represents the flux front at 32 mT applied field, and the front visible as a brighter line, representing the front at 30 mT. The constant difference field region demonstrates the validity of the MS theory [3]: after saturation of the antidots there is a 2 mT increase of the field everywhere in that region of the sample but there is no difference between the interstitial and the antidots positions since the latter are saturated at their maximum value n_{sat}. However, the incommensurate 1-dimensional channels are clearly visible, vortices flow at higher density along those paths. The flux front is strongly influenced by the faster advancing vortices along those channels. Due to the higher penetration speed of those vortices the flux progresses farther at the position of the incommensurate channels increasing the roughness of the flux front. This effect can be indeed clearly observed in fig. 2, in particular in the most advanced front, at 32 mT. Note that the number of vortices per antidot increases smoothly to n_{sat} over a region of width of about five antidots.

The phenomena occurring in systems with hexagonal periodic arrays of pinning sites are by far more complex than with square arrays and up to now considerably less studied. One of the new features is already demonstrated in fig. 1(a), the advance of the field in channels along one preferential direction of the antidot triangular lattice. In numerical simulations on triangular lattices [14], however, the vortices move interstitially in the direction of the driving force, *i.e.* perpendicular to the edges of the sample. To clarify this point we performed an

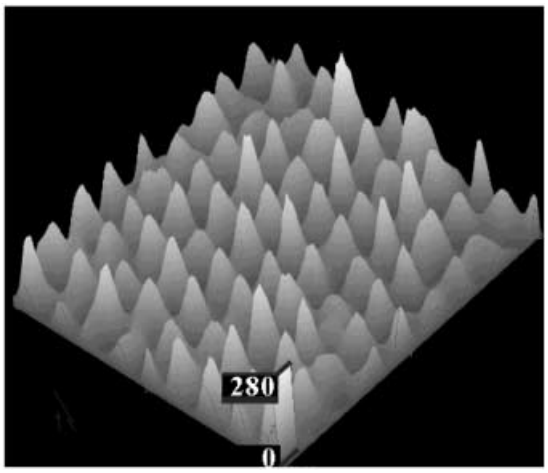

Fig. 4 – Field distribution obtained from the MO image recorded at 7 K in 0 T external field after a hysteresis loop to 1 T. The field is maximum at the position of the antidots. The scale for the height of the peaks is given in number of trapped vortices. Since the picture is constructed from the field image, the shape of the peaks indicates the local field profile in the sample.

experiment near the corner of the sample, where the dynamics of the flux entering from two perpendicular edges can be visualised, and where from theory and simulations we expect two perpendicular directions for vortex penetration. The resulting MO picture taken at $T = 7\,\mathrm{K}$ and applied field of 23 mT is shown in fig. 3. The channels of easy vortex penetration are visible for both edges of the sample, with an angle of 60° between each other and thus *not* perpendicular to the edges of the sample. It is important to notice that Reichhardt, Olson and Nori [14] observed in simulations on systems with square arrays of pinning sites that vortices move along the directions of the array.

The pinning properties of the antidots can be further investigated by analysing the remanent state of the vortex system when the applied field is decreased from above the total penetration field to 0 T. Figure 4 shows the 3D picture constructed from the image recorded at 7 K in 0 T external field, after an applied field of 1 T. Although figs. 1 and 2 are taken at 8 K, there is no essential difference between measuring at 7 K or 8 K, due to the weak temperature dependence of ξ and λ at low temperature. Also the temperature dependence of the critical current j_c and vortex pinning potential is very small in this interval. The scale for the height of the peaks in fig. 4 is given in number of trapped vortices. The experiment clearly shows the almost absence of field in interstitial positions. This suggests that on the down-going curve of a hysteresis loop, the first vortices to leak out from the sample are the interstitial vortices, while the multi-quanta vortices apparently remain still pinned at the antidots. This presents additional evidence of the strong pinning properties of the antidot lattice: the pinning by it is stronger than the intrinsic strong pinning of the $YBa_2Cu_3O_7$ film at 7 K.

In conclusion, we find that the amount of trapped flux in these large antidots is in suprising agreement with the Mkrtchyan and Schmidt [3] theory. The flux is observed to penetrate preferentially along the antidot lattice vectors. Both "channeling" along certain preferred rows and hopping between channels is observed, in agreement with numerical simulations.

This study is also relevant for the improvement of SQUIDs. Due to their extreme sensitivity to small magnetic fields and field gradients, SQUIDs are becoming increasingly popular in applications ranging from magneto-cardiography to the detection of gravity waves. One of

the key limitations still present is the noise generated by the SQUID itself due to moving vortex lines in the superconducting material of the SQUID structure. Recently, some of us [19, 20] have succeeded in a significant reduction of this noise by the introduction of antidots on a periodic lattice in the superconducting material forming the SQUID loop. Our present high-resolution magneto-optics provides a valuable tool in studying such a superconducting system and can lead to further noise reduction in superconducting devices.

* * *

We thank Dr. M. Pannetier and J. M. Huijbregtse for interesting suggestions. This work is part of the research program of the Stichting Fundamenteel Onderzoek der Materie (FOM), which is financially supported by the Nederlandse Organisatie voor Wetenschappelijk Onderzoek (NWO).

REFERENCES

[1] Civale L., Marwick A. D., Worthington T. K., Kirk M. A., Thompson J. R., Krusin-Elbaum L., Sun Y., Clem J. R. and Holtzberg F., *Phys. Rev. Lett.*, **67** (1991) 648; Blatter G., Feigel'man M. V., Geshkenbein V. B., Larkin A. I. and Vinokur V. M., *Rev. Mod. Phys.*, **66** (1994) 1125.
[2] Dam B., Huijbregtse J. M., Klaassen F. C., van der Geest R. C. F., Doornbos G., Rector J. H., Testa A. M., Freisem S., Aarts J., Martinez J. C., Stäuble-Pümpin B. and Griessen R., *Nature*, **399** (1999) 439.
[3] Mkrtchyan G. S. and Schmidt V. V., *Sov. Phys. JETP*, **34** (1972) 195.
[4] Rossel E., van Bael M., Baert M., Jonckheere R., Moshchalkov V. V. and Bruynseraede Y., *Phys. Rev. B*, **53** (1996) R2983.
[5] Metlushko V. V., DeLong L. E., Baert M., Rossel E., van Bael M., Temst K., Moshchalkov V. V. and Bruynseraede Y., *Europhys. Lett.*, **41** (1998) 333.
[6] Moshchalkov V. V., Baert M., Metlushko V. V., Rossel E., van Bael M. J., Temst K., Jonckheere R. and Bruynseraede Y., *Phys. Rev. B*, **54** (1996) 7385.
[7] Moshchalkov V. V., Baert M., Metlushko V. V., Rossel E., van Bael M. J., Temst K., Bruynseraede Y. and Jonckheere R., *Phys. Rev. B*, **57** (1998) 3615.
[8] Baert M., Metlushko V. V., Jonckheere R., Moshchalkov V. V. and Bruynseraede Y., *Phys. Rev. Lett.*, **74** (1995) 3269.
[9] Moshchalkov V. V., Baert M., Rossel E., Metlushko V. V., van Bael M. and Bruynseraede Y., *Physica C*, **282-297** (1997) 379.
[10] Bruynseraede Y., Puig T., Rossel E., Baert M., van Bael M., Temst K., Moshchalkov V. V. and Jonckheere R., *J. Low Temp. Phys.*, **106** (1997) 173.
[11] Metlushko V., Welp U., Crabtree G. W., Zhao Zhang, Brueck S. R. J., Watkins B., DeLong L. E., Ilic B., Chung K. and Hesketh P. J., *Phys. Rev. B*, **59** (1999) 603.
[12] Reichhardt C. and Nori F., *Phys. Rev. Lett.*, **78** (1997) 414.
[13] Reichhardt C., Olson C. J. and Nori F., *Phys. Rev. B*, **57** (1998) 7937.
[14] Reichhardt C., Olson C. J. and Nori F., *Phys. Rev. B*, **58** (1998) 6534.
[15] Reichhardt C. and Nori F., *Phys. Rev. Lett.*, **82** (1999) 414.
[16] Koblischka M. R. and Wijngaarden R. J., *Supercond. Sci. Technol.*, **8** (1995) 199.
[17] Castellanos A., Wördenweber R., Ockenfuss G. and v.d. Hart A., *Appl. Phys. Lett.*, **71** (1997) 962.
[18] Schneider J., Kohlstedt H. and Wördenweber R., *Appl. Phys. Lett.*, **63** (1993) 2426.
[19] Selders P., Castellanos A. M., Vaupel M. and Wördenweber R., *IEEE Trans. Appl. Supercond.*, **9** (1999) 2967.
[20] Selders P., Castellanos A. M., Vaupel M. and Wördenweber R., *Appl. Supercond.*, **5** (1997) 269.